Spectrochimica Acta Part A: Molecular and Biomolecular Spectroscopy 296 (2023) 122650

Contents lists available at ScienceDirect

Spectrochimica Acta Part A: Molecular and Biomolecular Spectroscopy

journal homepage: www.journals.elsevier.com/spectrochimica-acta-part-a-molecular-and-biomolecular-spectroscopy

Influence of cadmium ion on denaturation kinetics of hen egg white-lysozyme under thermal and acidic conditions

Liming Liu [a], Xinfei Li [a], Ning Chen [a], Xiaodong Chen [a], Lei Xing [b,*], Xiaoguo Zhou [a,*], Shilin Liu [a,*]

[a] Department of Chemical Physics, University of Science and Technology of China, Hefei 230026, China
[b] State Key Laboratory of Analytical Chemistry for Life Science, School of Chemistry and Chemical Engineering, Nanjing University, Nanjing 210023, China

HIGHLIGHTS

- Cd^{2+} promote the direct formation of ordered β-sheets from the uncoiling of α-helices by skipping intermediate structure.
- Cd^{2+} induce protein denaturation to form gels rather than amyloid fibrils, along with the "off-pathway".
- A combined interaction of Cd^{2+} and acid is confirmed in the transformation of tertiary and secondary structures of HEWL.

GRAPHICAL ABSTRACT

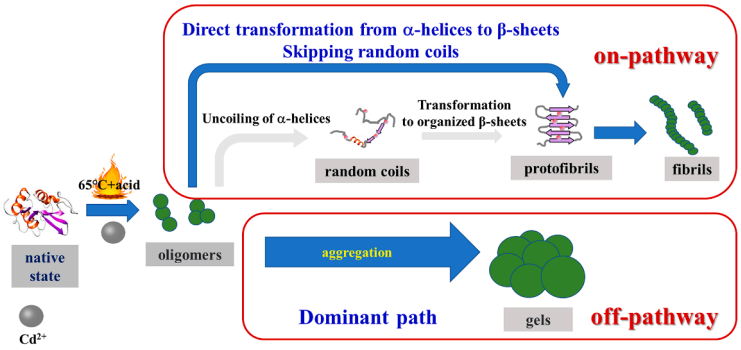

ARTICLE INFO

Keywords:
Protein denaturation
Raman spectroscopy
Kinetics
Cadmium
Lysozyme

ABSTRACT

To study the influence of Cd(II) ions on denaturation kinetics of hen egg white lysozyme (HEWL) under thermal and acidic conditions, spontaneous Raman spectroscopy in conjunction with Thioflavin-T fluorescence, AFM imaging, far-UV circular dichroism spectroscopy, and transmittance assays was conducted. Four distinctive Raman spectral markers for protein tertiary and secondary structures were recorded to follow the kinetics of conformational transformation. Through comparing variations of these markers in the presence or absence of Cd (II) ions, Cd(II) ions show an ability to efficiently accelerate the disruption of tertiary structure, and meanwhile, to promote the direct formation of organized β-sheets from the uncoiling of α-helices by skipping intermediate random coils. More significantly, with the action of Cd(II) ions, the initially resulting oligomers with disordered structures tend to assemble into aggregates with random structures like gels more than amyloid fibrils, along with a so-called "off-pathway" denaturation pathway. Our results advance the in-depth understanding of corresponding ion-specific effects.

* Corresponding authors.
E-mail addresses: xl1992@nju.edu.cn (L. Xing), xzhou@ustc.edu.cn (X. Zhou), slliu@ustc.edu.cn (S. Liu).

https://doi.org/10.1016/j.saa.2023.122650
Received 6 January 2023; Received in revised form 11 March 2023; Accepted 17 March 2023
Available online 23 March 2023

1. Introduction

Specific three-dimensional structures are essential for distinct physiological functions of proteins [1,2]. Under stressful conditions, proteins can undergo structural changes and self-assemble into aggregates like amyloid fibrils (so-called "on-pathway") and gels ("off-pathway"). Among these aggregates, the amyloid fibrils with highly ordered β-sheet-rich structures are well-known to associate with some neurodegenerative diseases, such as Alzheimer's disease (AD), Parkinson's syndrome and amyotrophic lateral sclerosis [3–5]. Thus, in-depth understanding of supramolecular structures and amyloid fibrillation mechanisms has great implications for the treatment of diseases [6,7].

For the sake of simplicity and economy, a model protein, hen egg white lysozyme (HEWL), is commonly chosen as a representative for amyloid fibrillation studies. It is reasonable because its structure is not only highly homologous to human lysozyme, but also the active site is similar to the sequence of amyloid-β (Aβ) peptides (AD related peptides) [8]. Extensive investigations were performed for amyloid fibrillation of HEWL in thermal conditions [9], together with various chemicals like acid [10], O-methylated 3HPs [11], fluoroquinolone drug ofloxacin [12], and succinimide [13]. Beyond these factors, increasing evidences have proved that metal ions can also induce protein denaturation in aqueous medium, which is well-known as "Hofmeister series" according to the sequence of their action strength, since their accumulation around brain plaques of AD patients was observed [14–19]. Accordingly, they have attracted widespread interest as potentially pathogenic factors. The specific roles (an inhibitor or a promoter) of several endogenous metal ions, such as Cu^{2+} [20], Zn^{2+} [21], Mg^{2+} [22], and Al^{3+} [22,23], were proposed on protein amyloid fibrillation. For instance, a double-edged role has been verified recently for Al(III) ions in the amyloid fibrillation of lysozymes [23], that in addition to postponing α-helix degradation, Al(III) ions accelerate conformational transformations from α-helices to organized β-sheets.

As an exogenous heavy metal ion, Cd(II) ion plays a considerable role in environmental, food, biological, and medical fields [24–28]. As a relatively high cadmium level was detected in plasma, brain and liver of AD patients,[24,29–32] cadmium exposure was also thought to pose a risk for AD. For elucidating the influence of Cd(II) ions on protein structures and amyloid fibrillation mechanisms, some experimental studies were carried out. Using fluorescence spectroscopy, isothermal titration calorimetry, molecular docking and dynamics simulation, Wang et al. located three thermodynamic identical binding sites for Cd (II) ions on lysozyme, and a slightly altered secondary structure was suggested due to interaction from the metal ions [33]. Their conclusion was contrary to Olmo et al.'s result [34] that only variations in the conformation of lysozyme were observed without a visible change on the secondary structure. The association between Aβ peptide aggregation and cigarette-related compounds, such as nicotine, polycyclic aromatic hydrocarbons, and metal ions, Cd(II), Cr(III), Pb(II), and Pb(IV), was monitored using AFM imaging, NMR, fluorescence assay, and mass spectrometry [35], in which the Cd(II) ions showed a capability of altering the Aβ aggregation pathway, that is, amorphous Aβ aggregates were favorably formed in the presence of Cd(II) rather than conventional Aβ fibrils. A further phenomenon was observed in the Aβ42 aggregation process, that the formation of high-molecular-weight aggregates was more favorable in the presence of Cd(II) ions [24,36]. Furthermore, Jiang et al. [37] investigated the impacts of Cd(II) ions on the conformation and self-aggregation of Alzheimer's tau peptide *R*3. The ThS fluorescence assays indicated that Cd(II) ions accelerated heparin-induced or independently induced *R*3 aggregation. In addition, the α-helical structure on peptide chain was increased with the action of Cd(II), and the resulting *R*3 filaments became much smaller [37]. The similar effect was also observed in the aggregation of α-Synuclein [38] and cytosolic proteins [39]. Especially in the nucleation stage in the amyloid formation process, cadmium-aggregated proteins formed seeds for the misfolding of other proteins. Notably, these above studies were mainly focused on the influence of Cd(II) ions on morphology and structures of the end-formed aggregates, and their action mechanisms on the denaturation kinetics of lysozyme was unclear. This gives us a motivation to clarify the specific action of Cd(II) ions on different kinetic stages of protein denaturation process.

Because the Cd(II)-induced denaturation process of HEWL under physiological conditions is very slow, a relatively stressful condition of thermal (65 °C) and acidic (*p*H 2.0) treatment is chosen hereby. The corresponding mechanisms and kinetics of the HEWL amyloid fibrillation are well-studied with the absence of Cd(II) ions [10,40–43]. Spontaneous Raman spectroscopy, a label-free, nondestructive, and powerful analytical technique, is used to detect the secondary and tertiary structure transformation of protein at the molecular level [9,44–47]. Thioflavin-T (ThT) fluorescence spectroscopy, AFM imaging, far-UV circular dichroism (CD) spectroscopy, and transmittance measurements are also performed to verify the changes of molecular conformation and morphology in the HEWL denaturation process. As a result, the specific influence of Cd(II) ions on the transformation of protein tertiary and secondary structures, as well as the formation of gel-like aggregates along the "off-pathway", is derived from comparing the results in the absence and presence of Cd(II) ions. Our conclusions will provide valuable information for understanding the molecular mechanism of ion-specific effects in protein structures in aqueous environment and for studying the toxic effects of exogenous ions.

2. Experimental methods

2.1. Solution preparation

HEWL (activity ≥ 20000 U/mg, A610308-0005) in the native state and $CdCl_2{\cdot}2.5H_2O$ were purchased from Sangon Biotech and Sinopharm Chemical Reagent, and used without further purification. The initial concentration of HEWL was 20 mg/mL in aqueous solution. To compare the influence of Cd(II) ions, two solutions were prepared, i.e. one without Cd(II) ions, and the other with the 20:1 M ratio of Cd(II) ions to HEWL. Then the two solutions were adjusted to *p*H = 2.0 with hydrochloric acid, and then the solutions in sealed glass vials (4 ml) were incubated in a thermoshaker at 65 °C without agitation for more than 200 h. Actually, in the absence of metal ions, this thermal and acidic treatment were well-studied for amyloid fibrillation kinetics of lysozymes previously [10]. In addition, chloride ions have very little influences on protein structures, as indicated previously [48,49]. At various incubation times, aliquots of the denaturing protein solution were taken from the vials. Subsequently, a centrifugation at 12,000 g was performed for 20 min to separate gelatinous phase. The residual supernatant was used for Raman spectroscopy, ThT fluorescence assays, far-UV CD spectroscopy, AFM imaging and transmittance measurements. As concluded previously [50], a small amount of aggregates, such as gels and fibrils, remain in the supernatants, thus all spectral features of protein and its denaturation products like protofibrils and gel-like aggregates can be detected in the Raman spectra, ThT fluorescence assay, CD spectroscopy, and transmittance analyses of the supernatant [23]. In addition, the morphologies of oligomers and amyloid fibrils can be clearly observed by using AFM imaging.

2.2. Spontaneous Raman spectroscopy

Spontaneous Raman spectroscopy was measured as described previously [10,13,23]. Briefly, sample solutions were stored in a 10 mm × 10 mm quartz cuvette at the set temperature. A continuous laser (Verdi V5, Coherent) with a power of 4 W at 532 nm was used as the excitation light source. Scattered light was collected, dispersed and recorded by a triple monochromator (TriplePro, Acton Research) with a liquid–nitrogen-cooled CCD detector (Spec-10:100B, Princeton Instruments). The resolution of present Raman spectra was ~ 1 cm^{-1} in the frequency range of 200–3000 cm^{-1}, and the wavelength was carefully calibrated

using standard spectral lines from a mercury lamp. The acquisition time for each measurement was 1 min, and the reported Raman spectra were averaged for 10 acquisitions under the same conditions for better signal-to-noise ratios. In addition, the Raman spectra were corrected by subtracting the spectra of water with Cd(II) ions measured under identical conditions. Therefore, sufficiently reliable spectra were provided in present study.

2.3. ThT fluorescence assays

During the denaturation process, 0.5 ml of supernatant taken at different incubation times was added into 4.5 ml of ThT solution (the concentration of 12 mg/L). Steady-state fluorescence emission spectra of the mixed solutions were recorded using a multi-purpose fiber optic spectrometer (AvaSpec-ULS2048, Avantes), with photo-excitation at 409 nm. The wavelength range of the spectra covered from 400 to 800 nm, and the emission intensity at 477 nm was used as an indicator of fluorescence intensity.

2.4. Far-UV circular dichroism spectroscopy

The supernatant was diluted 100-fold. The far-UV CD spectra of the samples in 2 mm quartz cuvettes were measured using a CD spectrophotometer (J-1700, JASCO) in the wavelength range of 195–250 nm, with a bandwidth of 1.0 nm. The scanning speed was 100 nm/min, and the response time was 1 s. To ensure the accuracy, at least three independent measurements were completed and the averaged spectral data were reported.

2.5. Atomic force microscopy (AFM) imaging

All AFM images were acquired on air-dried samples using a Dimension Icon scanning probe microscope from Bruker in tapping mode. A 5 μm × 5 μm scanner was used in the experiments. The supernatant was diluted 10 times with Milli-Q water and then dropped onto a freshly cleaved mica. Fifteen minutes later, the protein solution was rinsed off with deionized water three times. The mica surface was dried at room temperature, and the sample was stored in a desiccator. The AFM images were represented using an open-access software from Nanoscope Inc.

2.6. Transmittance measurement

A commercial UV–vis spectrometer (UV-2550, Shimadzu) was used to measure light transmittance of the supernatant at different incubation times. The absorption wavelength range was 300–500 nm. Compared with the native HEWL, a weak shoulder peak appeared at the red-side and extended to more than 450 nm after denaturation. Apparently, this shoulder is contributed by the formed aggregates. According to the Beer-Lambert law, the change in solution transmittance at ~ 380 nm can directly reflect the relative proportion of the formed aggregates.

3. Results and discussion

3.1. Morphologies of HEWL in the denaturation process

Fig. 1 shows morphological changes of proteins during denaturation process recorded at three representative incubation times, with thermal/acid or thermal/acid/Cd(II) treatments. Similar to the previous study [10], some oligomers appear in the initial incubation stage in the absence of Cd(II) ions (Fig. 1a). Overt time, the number of oligomers gradually increases (Fig. 1b) and assembles into protofibrils and mature fibers with small amounts of gel-like aggregates with disordered structure (Fig. 1c). In contrast, with the action of Cd(II) ions, the formation of protofibrils is significantly advanced. As shown in Fig. 1d and 1e, protofibrils with a length of a few microns are clearly observed after incubation for 24 h, and they become more dense and intertwined with each other with time. To our surprise, much less mature fibers are produced after incubation for 192 h in the presence of Cd(II) ions (Fig. 1f). Moreover, the morphologies of the end-formed aggregates in Fig. 1f appear softer, indicating that more aggregates with disordered structures may be produced with the action of Cd(II).

It is well-known that with unfolding of tertiary and secondary structures, protein can assemble to form gel-like aggregates or amyloid fibrils along with “off-pathway” or “on-pathway”, respectively [23].

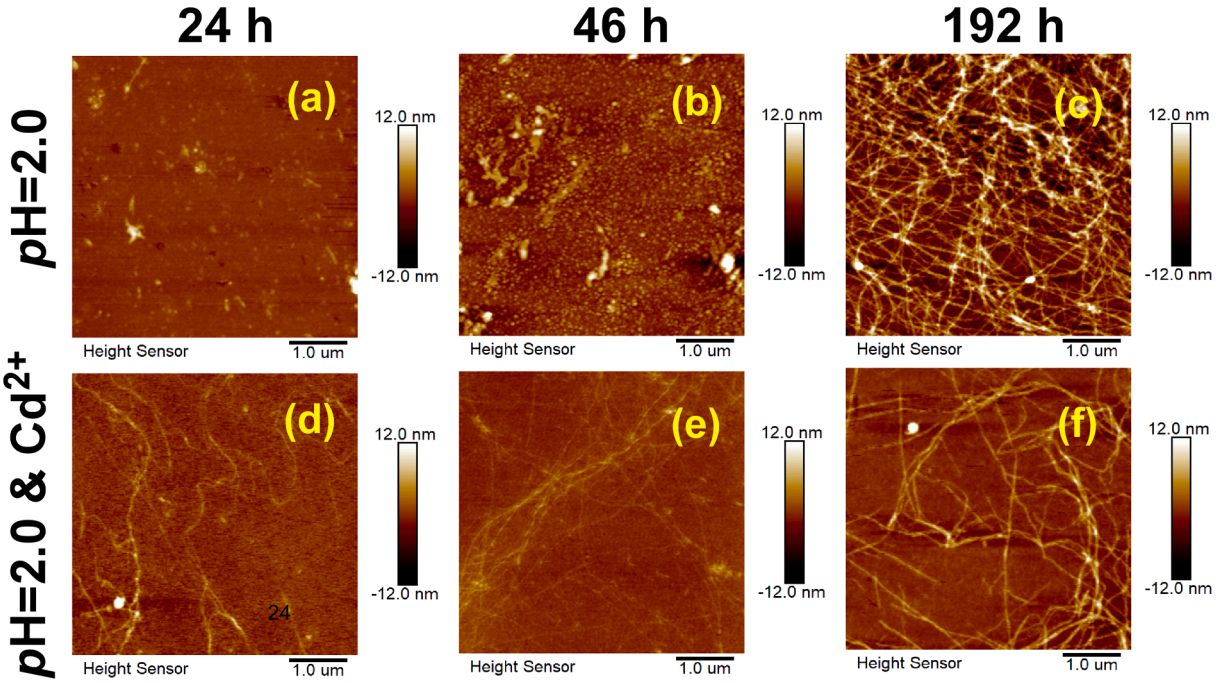

Fig. 1. AFM height images of HEWL incubated under thermal/acid conditions for (a) 24 h, (b) 46 h and (c) 192 h, and under thermal/acid/Cd(II) conditions for (d) 24 h, (e) 46 h and (f) 192 h.

According to the fact that different aggregation forms should have different light transmission, the gels and fibrils show translucent (or opaque) and hence their formation will cause the change of the supernatant transmittance. Thus, we can easily infer the formation rates of the aggregates by recording transmittance of the supernatant at each specific incubation time, although we could not directly observe the formed oligomers in solution with naked eyes. As shown in Fig. 2, the change rate of solution transmittance is very close during the first few hours regardless of the presence of metal ions, indicating that Cd(II) ions have insignificant effects on the formation of insoluble oligomers in comparison to acid. It is inconsistent with the acceleration effect observed in the nucleation step of α-Synuclein amyloid formation process [38]. However, the formation rate of large-size aggregates is obviously accelerated with the action of Cd(II) ions. As a result, a large amount of opaque gel-like aggregates with irregular shapes are produced with the adding of Cd(II) ions, as shown in the inserted photos of Fig. 2. These results verify the facilitating effect of Cd(II) ions on the gel-like formation along "off-pathway" from the oligomers, which agrees with the previous conclusions in the Aβ aggregations [35,36].

3.2. Raman spectra of native lysozyme and its final-state aggregates

Although there are visible differences in the formation rate of gel-like aggregates in the absence and presence of Cd(II) ions, the morphology of the end-produced aggregates are difficultly distinguished with naked eyes, except for quantity. Herein, spontaneous Raman spectroscopy was performed to real-time detect the molecular structure of protein. Fig. 3 shows the Raman spectra of the native HEWL and the end-formed aggregates including fibrils and gels in the supernatant, with thermal/acidic and thermal/acidic/Cd(II) treatments. Notably, along with the formation of fibrils and gel-like aggregates, the protein concentration in the supernatant monotonously decreases during incubation, resulting in the weakened intensities of all Raman peaks during incubation. Thus, as suggested by the previous studies [51–53], we used the spectral intensity of the Phe ring at 1003 cm^{-1} to normalize all band intensities in Fig. 3, since this peak is insensitive to microenvironment and dominantly depends on protein concentration. For the sake of simplicity, we chose four well-known vibrational bands as Raman indicators for tertiary and secondary structures of protein in the following discussions.

As listed in Table 1, two vibrational bands contributed by Trp residues on protein side chain are used to monitor changes of protein tertiary structure, i.e. the peak at 759 cm^{-1} and the double peaks at 1340 and 1360 cm^{-1}. The former is contributed by coupled vibrations of the in-phase symmetric ring breathing of benzene and pyrrole rings of Trp residue [54–56], and its full-width half-maximum (FWHM) is sensitive to conformational distributions of Trp in side chain microenvironments. The double peaks at 1340 and 1360 cm^{-1} are attributed to the Fermi resonances comprising of a fundamental in-plane C8-N1 stretching and a combination of out-of-plane deformations of indole rings of Trp [57–59]. The intensity ratio of this doublet, I_{1340}/I_{1360}, is very sensitive to the hydration degree of Trp residue [60]. Once the indole ring of Trp is exposed to aqueous medium, the I_{1340}/I_{1360} ratio is larger than 1.0. Conversely, a hydrophobic environment surrounds the indole ring of Trp. Therefore, these two markers are both widely used to indicate the changes of side chain microenvironments with the break of protein

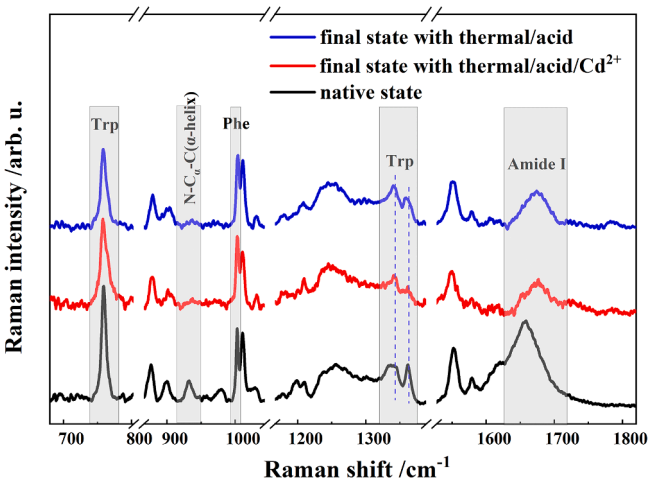

Fig. 3. Raman spectra of the native HEWL (in black) and the final states formed with the thermal/acid (in blue) and thermal/acid/Cd(II) (in red) treatments. The Raman markers for protein structures discussed in text are marked with grey boxes.

Table 1
Parameters and assignments of Raman vibrational bands of HEWL used in the discussions.

amino acid residues	protein structure	Raman shift/cm^{-1}	Assignment	Raman markers
Trp	tertiary	759	coupled vibrations of in-phase breathings of benzene and pyrrole	FWHM[54-56]
Trp	tertiary	1340/1360	Fermi resonances between the fundamental in-plane N1 = C8 stretching and the combination bands of ring out of plane deformations	I_{1340}/I_{1360}[57-60]
N-C_α-C	secondary	932	stretching of N-C_α-C segment in α-helical structures	intensity[54, 56]
amide I	secondary	1640–1650 1650–1660 1660–1670 1670–1680	random coils α-helices β-sheets random structures, β turn	peak position [10, 51, 61-64]

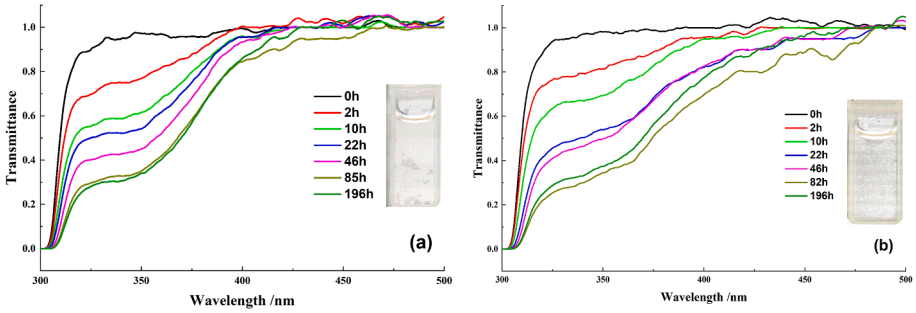

Fig. 2. UV–vis absorption spectra of the HEWL solution at different incubation times with thermal/acid (a) and thermal/acid/Cd(II) (b) treatments, where the photos of the end-formed aggregates after denaturation were inserted.

tertiary structures. As shown by the magnified spectra in Fig. 4a and 4b, the FWHM at 759 cm^{-1} and the I_{1340}/I_{1360} ratio are visibly varied after denaturation, indicative of the microenvironment changes as well as the destruction of protein tertiary structures.

For the protein skeleton, another two bands are commonly used to trace transformation of the secondary structures, i.e. the N-C_α-C peak at 932 cm^{-1} and the amide I band (1640–1680 cm^{-1}). Notably, the peak at 932 cm^{-1} is well-known to be contributed by the N-C_α-C stretching vibration of α-helical structures [54,56]. As shown in Fig. 5a, its intensity is approximately completely reduced in the end-produced aggregates, indicating that the α-helical structures in the native HEWL are almost fully destroyed. The amide I band is assigned to the coupling mode of the C═O and C—N stretching vibration and a small amount of N—H in-plane bending vibration [51]. It is widely used to monitor the transformation from α-helices to β-sheets, since the relative strengths of hydrogen bonding interactions (C═O…H) between amide groups and dipole–dipole interactions between carboxyl groups are varied in different secondary structures. As listed in Table 1, for HEWL α-helices usually have low-frequency accordion-like motions with the frequency at 1650–1660 cm^{-1} [61], organized β-sheets contribute the vibrational intensity at 1660–1670 cm^{-1} [10], and the frequencies of disordered structures, such as random coils and β-turns, are lower than 1650 cm^{-1} or higher than 1670 cm^{-1} [62–64]. Compared with that of the native HEWL, the amide I band of the final aggregates exhibits a blue shift of ~ 15 cm^{-1} as shown in Fig. 5b, indicating transformation of the α-helices to the other conformations, such as β-sheets or random structures, during protein denaturation.

3.3. Evolutionary kinetics of HEWL tertiary structures

To uncover the influence of Cd(II) ions on the evolutionary kinetics of HEWL tertiary structures, incubation time-dependent curves of the FWHM at 759 cm^{-1} and the I_{1340}/I_{1360} ratio under thermal/acid and thermal/acid/Cd(II) conditions were measured and directly compared. As shown in Fig. 4d, the I_{1340}/I_{1360} ratio of Trp increases monotonically with incubation time in both experimental conditions and converges to equilibrium after 70–100 h, indicating that the unfolding of tertiary structures proceeds immediately upon being incubated. Moreover, although the curves both show typical 1st-order reaction characteristics of single exponential growth, the change rate is apparently accelerated in the presence of Cd(II) ions, verifying the promoting effect of Cd(II) on the exposure of Trp residues on side chains.

In comparison to the above I_{1340}/I_{1360} marker, the kinetic curves of the FWHM indicator show different pattern. Although the broadening of this peak at 759 cm^{-1} is moderately accelerated in the presence of Cd(II) ions, as shown in Fig. 4c, it is obvious that the change rate of the Trp FWHM is much slower than that of the I_{1340}/I_{1360} marker, and especially in the later incubation stage (greater than100 h), this FWHM indicator continues to grow. Considering that this peak width is an indicator for conformational distributions of Trp, the wider FWHM (Fig. 4c) implies that more free conformations of Trp residue are formed with the influence of Cd(II) ions. It is worth noting that the dominant self-assemble process of HEWL changes to the "off-pathway" from oligomers to gel-like aggregates under thermal/acid/Cd(II) treatment. In these gel-like aggregates, random structures are predominant for protein secondary structures rather than organized β-sheets (Fig. 6). Hence, we can imagine, the mean interaction between Trp residue and surrounding microenvironment is much weakened in gel-like aggregates, leading to the formation of more various rotational isomers. That is, Trp residues on side chains have the higher degree of freedom in gels with disordered molecular structures.

3.4. Transformation kinetics of HEWL secondary structures

Fig. 5a and 5b show the magnified Raman spectra of the native HEWL (in black) and the end-formed aggregates (in red) in the range of 720–800 cm^{-1} (N-C_α-C stretching peak) and 1315–1380 cm^{-1} (amide I band), respectively. The incubation time-dependent curves of these two indicators under thermal/acid (in black) and thermal/acid/Cd(II) (in red) conditions are plotted in Fig. 5c and 5d. Apparently, the two markers show sigmoid functional relationships on incubation time with thermal and acidic treatments, which is greatly consistent with our previous results [10]. By fitting these curves with a sigmoid function of the equation (1) [65–67], we can obtain the corresponding kinetic parameters,

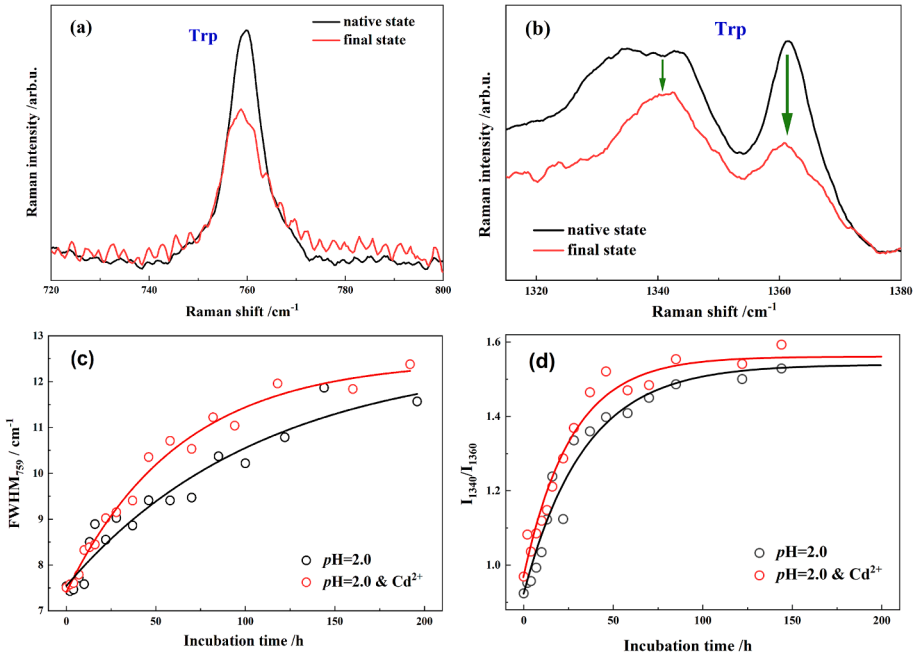

Fig. 4. Magnified Raman spectra of the native HEWL (in black) and the final state (in red) in the range of 720–800 cm^{-1} (a) and 1315–1380 cm^{-1} (b); and incubation time-dependence curves of the FWHM at 759 cm^{-1} (c) and the I_{1340}/I_{1360} ratio (d) under thermal/acid (in black) and thermal/acid/Cd(II) (in red) conditions.

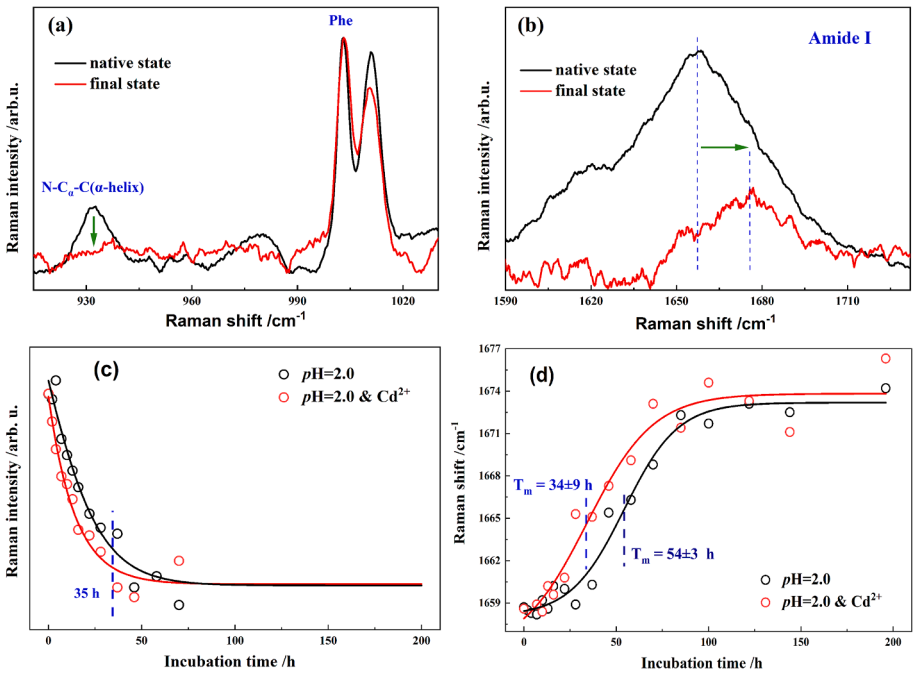

Fig. 5. Magnified Raman spectra of the native HEWL (in black) and the final state (in red) in the range of 915–1030 cm^{-1} (a) and 1590–1730 cm^{-1} (b); and incubation time-dependence curves of the intensity at 932 cm^{-1} (c) and the peak position of amide I band (d) under thermal/acid (in black) and thermal/acid/Cd(II) (in red) conditions.

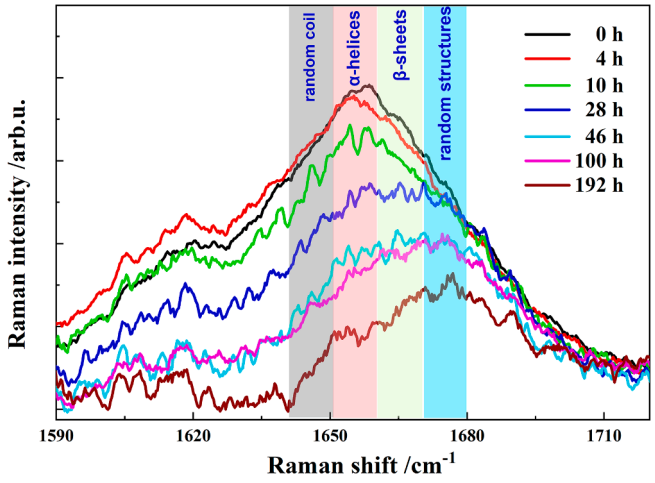

Fig. 6. Time-dependent Raman spectra of the amide I region, where the intensities were normalized by the Phe peak at 1,003 cm^{-1}.

$$F = F_D + \frac{F_N - F_D}{1 + exp[(T - T_m)/\Delta T]} \quad (1)$$

where F_N and F_D correspond to the indicator values like FWHM, fluorescence intensity, or Raman shift of initial and final states, respectively, T denotes incubation time, T_m is the transition midpoint time, and $2\times\Delta T$ can reflect the transition interval.

During the earliest kinetic stage (0–10 h), the oligomers with disordered structures are formed with the unfolding of protein tertiary structures, in which a large proportion of aromatic amino acid residues on side chains (like Trp) are exposed to border regions of the protein. The uncoiling of α-helices occurs immediately under the influence of hydrogen bonds from nearby water, resulting in the significantly decreased N-C_α-C intensity. Additionally, there is a lag phase between the uncoiling of α-helices and the formation of organized β-sheets, as indicated by comparison of the two black curves in Fig. 5c and 5d. As proposed previously [10], the statistical coils of disordered structure are preferred to be formed as intermediates from the transformation of α-helices, prior to the formation of β-sheets. The midpoint transition time T_m is determined to be 54 ± 3 h under the present conditions (Fig. 5d), which obviously lags behind the uncoiling of α-helices (~35 h as noted with a blue-colored dash line in Fig. 5c).

In comparison to the kinetics in the absence of Cd(II) ions (black traces in Fig. 5c and 5d), the lag phases of the two spectral markers are both significantly shorter in the presence of the metal ions, whereas the transformation rates (i.e. slopes in the growth phases) remain. Notably, the characteristic rates of the I_{1340}/I_{1360} ratio of Trp (Fig. 4d) and the N-C_α-C intensity (Fig. 5c) are very close, thus we can imagine that Cd(II) ions efficiently induce the uncoiling of α-helices, accompanying with the exposure of Trp residues. More importantly, the midpoint transition time (T_m) of the amide I peak position is determined to be 34 ± 9 h in the presence of Cd(II) ions as shown in Fig. 5d, which is obviously shifted ahead in comparison to that without the Cd(II) ions. As this time is less than the full destruction time of α-helices,[13] organized β-sheets are expected to be immediately formed with the uncoiling of α-helices, by skipping the formation of intermediate random coils.[13,68] Actually, the promoted formation of protofibrils in the AFM images (Fig. 1d and e) undoubtedly supports this conclusion. All these evidences demonstrate that the influence of Cd(II) leads to approximately simultaneous changes in protein secondary and tertiary structures.

As mentioned above, the whole band of amide I includes the contributions of several conformations, such as α-helices, β-sheets, random coils and other random structures like β-turns. Thus, the marker of peak position cannot reflect all information of transformations among these isomers. To exhibit the detailed population change of protein secondary structures and verify the most favorable aggregate pathway in the presence of Cd(II) ions at the molecular level, we plot the incubation time-dependent spectral profile within the amide I region in Fig. 6. The complicated change of band profile can be readily observed hereby during the HEWL denaturation with thermal/acid/Cd(II) treatment.

As shown with colored panels in Fig. 6, the whole band of amide I peak basically includes the contributions of four representative secondary structures. Apparently, the α-helices is dominant for the native

HEWL as well as a certain amount of β-sheets, corresponding to the peak position at 1658 cm^{-1}. Along the incubation process, the peak profile is initially broadened. The relative population of random coils is increased during the first incubation period (0–10 h), for example, as shown by the red curve in Fig. 6. Subsequently, the contributions of β-sheets and random structures are both improved with the reduction of α-helices, leading to a flat broad peak profile such as those profiles at 28, 46 and 100 h in Fig. 6. Notably, the relative intensity of β-sheets reaches a maximum at ~ 46 h, which is consistent with the protofibrils observed in the AFM images (Fig. 1e). This spectral change agrees with the transformation from the oligomers with disordered structures to the organized β-sheets. Subsequently, the relative population of random structures continues to grow during the overall incubation period and become the most dominant component after 100 h (Fig. 6), which is exactly consistent with the conclusion of "off-pathway to form gel-like aggregates" with the thermal/acid/Cd(II) treatment. Using the multi-component amide I Raman band fitting analysis,[56] the relative content of different secondary structures at various incubation times are obtained as shown in Fig. S1, and the relative population data are summarized in Table 2. Along with incubation time, the β-sheets are initially formed with the decrease of α-helices, then gradually slightly reduce, and simultaneously a great number of random structures are finally produced in end-formed aggregates. Apparently, these quantitative results further validate the above conclusion of Fig. 6.

Additionally, it is well-known that ThT fluorescence is the gold standard for quantification of the formation of cross β-sheet-rich structures during amyloid fibrillation [69–71]. At the molecular level, when a ThT molecule binds to intermolecular β-sheets of proteins, free rotations of the carbon–carbon bond between benzothiazole moiety and dimethylaniline unit are hindered, leading to the enhancement of its fluorescence emission [70]. Herein, we also performed ThT fluorescence assays for studying the influence of Cd(II) ions on the organized β-sheets formation kinetics, and further verifying our above conclusions of transformation of protein secondary structure. With the proceeding of protein denaturation, the β-sheets conformations are gradually formed as we expected, and the ThT fluorescence emission intensity at 477 nm shows a typical sigmoid functional curve with or without the presence of Cd(II) ions, as shown in Fig. 7.

By fitting the curves, the midpoint times (T_m) are determined to be 94 ± 4 h in the absence of Cd(II) and 42 ± 3 h with the adding of Cd(II), respectively. Under thermal and acidic conditions, the T_m value of ThT fluorescence kinetics is obviously later than that of the amide I marker (Fig. 5d), although both of them are thought to be indicators of protein secondary structures, especially α-helices and β-sheets. This relatively postponement has been also observed in our previous study [10]. We can imagine that the β-sheet-rich structure starts to be formed from statistical coils (such as oligomers close to molten ones) and quickly assembled during the transformation from amyloidogenic oligomers to fibrils, and hence its indicator, the ThT fluorescence intensity, is predominantly enhanced during the self-assembly period, while the frequency-shift of the amide I peak mainly occurs in the formation of statistical coils with random structures. Additionally, the fluorescence intensity is significantly enhanced after the 192 h incubation by 7-fold in the presence of Cd(II) ions and 12-fold without Cd(II), respectively. This inconsistent ThT fluorescence intensity in the final state under the two conditions agrees well with the fact that more gel-like aggregates are produced with thermal/acid/Cd(II) treatment, which is directly observed in the above AFM images and transmittance assays.

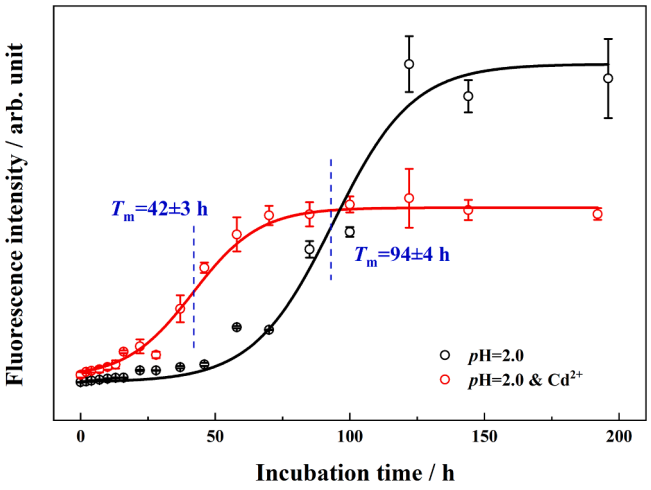

Fig. 7. Incubation time-dependent curve of ThT fluorescence emission intensity at 477 nm of the HEWL/ThT mixed solution, at two specific incubation times under thermal/acid and thermal/acid/Cd(II) conditions.

CD spectroscopy is another widely applied tool to investigate protein secondary structure changes. In a representative far-UV CD spectrum of protein in the wavelength range of 195–250 nm, the negative peaks at 208 and 222 nm are attributed to the α-helical structures, and the β-sheets have a strong contribution at 218 nm, while the random coils are located at 200 nm.[13,21,72] Thus, the relative population changes of these secondary structures can be derived from the CD spectroscopic analyses. Fig. 8 shows the far-UV CD spectra of HEWL in the native state and end-formed products. Apparently, the HEWL secondary structure is

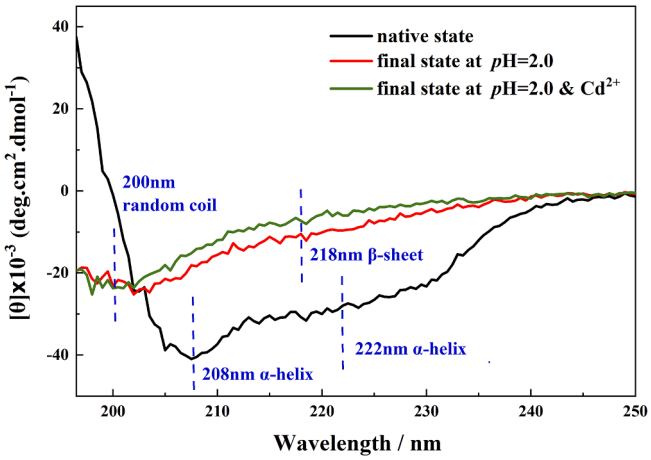

Fig. 8. Far-UV CD spectra of the native HEWL (in black) and the final states formed with the thermal/acid (in red) and thermal/acid/Cd(II) (in green) treatments. The locations of various protein secondary structures are marked with blue dashed lines.

Table 2
Curve fitting analysis of the amide I band profile at various incubation times (h) with the peak location (cm^{-1}) and the percentage component areas (A%).

Incubation time	Try		random coils		α-helix		β-sheet		random structures	
	peak	A%	peak	A%	peak	A%	peak	A%	peak	A%
0	1617	0.11	1640	0.19	1656	0.36	1669	0.21	1683	0.14
28	1617	0.08	1638	0.19	1655	0.31	1671	0.29	1683	0.13
46	1617	0.11	1638	0.14	1655	0.18	1672	0.46	1685	0.11
100	1617	0.12	1639	0.14	1654	0.11	1669	0.40	1683	0.23

significantly changed in both experimental conditions, since an obvious blue-shift was observed. Moreover, in the presence of Cd^{2+} ions the relative population of the random coils component in its denaturation products is increased as indicated by the enhanced blue-shift from 202 nm without the metal ions to 200 nm in thermal/acid/Cd^{2+} conditions. This conclusion is perfectly in line with the conclusions of Raman spectroscopy and ThT fluorescence assays.

3.5. Action mechanism of the Cd(II) ions on denaturation kinetics of HEWL

For the HEWL molecule in the native state, there are three most likely binding sites for Cd(II) ions according to electrostatic interaction. As Wang et al. proposed nnn, the first site is located on the protein surface, and the other two sites are located in the lumen of the molecule, in which the site 3 is the linkage to the Glu35 residue in the second α-helices. It is not difficult to imagine that these electrostatic forces have strong influence on hydrogen bonds, hydrophobic interactions, van der Waals forces and disulfide bonds among amino acid side chains, thus leading to the accelerated unfolding of the HEWL tertiary structures. Moreover, water molecules in solutions are more likely to enter the lumen according to electrostatic attraction of the metal ion, causing the disruption of this α-helical structure involving Glu35 residue. Hence, the lag phase of secondary structure transformation is rightfully shortened.

On the other hand, proteins can assemble into gel-like aggregates or amyloid fibrils along the “off-pathway” or “on-pathway” pathways, respectively. These two pathways usually compete in the protein denaturation process. As mentioned above, Cd(II) ions and Glu residues are tightly linked by electrostatic interactions. As a result, the direct transformation from α-helices readily occur with the action of Cd(II) ions, as indicated by the Raman marker of amide I. However, the electrostatic repulsion between the Cd(II) ions on amyloidogenic oligomers makes it difficult for self-assembly to occur in a specific direction, thus the “on-pathway” to form amyloid fibrils is significantly weakened. Instead, the gel-like aggregates along the “off-pathway” plays more dominant role in the HEWL denaturation kinetics with thermal/acid/Cd (II) treatments.

4. Conclusions

Uncovering the action mechanism of Cd(II) ions in denaturation kinetics of proteins is vital for understanding the essential relationship between metal ions and neurodegenerative diseases. Herein, we performed a joint experimental study of Raman spectroscopy, ThT fluorescence assays, AFM imaging and transmittance measurements on the denaturation kinetics of HEWL with thermal/acid and thermal/acid/Cd (II) treatments.

As shown by two Raman markers of Trp residue on protein side chains, the exposure of HEWL tertiary structures to aqueous medium is accelerated with the action of Cd(II) ions, and the self-assembly process from oligomers to gel-like aggregates, so-called “off-pathway”, is dominant in comparison to that in the absence of metal ions. Moreover, the transformation of HEWL secondary structures is significantly promoted under the combined interactions of Cd(II) and acid, i.e. organized β-sheets are formed immediately following the uncoiling of α-helices by skipping intermediate random coils. In addition, the experimental evidences clearly show that the initially produced oligomers tend to assemble into the aggregates with random structures like gels rather than the amyloid fibrils with the action of Cd(II) ions, which is consistent with the results of transmittance assays, ThT fluorescence and far-UV CD spectroscopy, and AFM images on the view of macroscopic. The downside is that the detailed mechanism of Cd(II) ions on the gel-phase formation at the molecular level is not clarified yet, due to the lack of structural data on oligomers. Further studies are undergoing to fill this information gap.

CRediT authorship contribution statement

Liming Liu: Writing – original draft. **Xinfei Li:** Investigation. **Ning Chen:** Software. **Xiaodong Chen:** Data curation. **Lei Xing:** Formal analysis. **Xiaoguo Zhou:** Supervision, Conceptualization, Project administration, Writing – review & editing. **Shilin Liu:** Supervision, Funding acquisition.

Declaration of Competing Interest

The authors declare the following financial interests/personal relationships which may be considered as potential competing interests: [Xiaoguo Zhou reports financial support was provided by National Natural Science Foundation of China. Lei Xing reports financial support was provided by China Postdoctoral Science Foundation.].

Data availability

Data will be made available on request.

Acknowledgements

This work was financially supported by the National Natural Science Foundation of China (Nos. 22073088, 21873089 and 22027801) and the China Postdoctoral Science Foundation (2019TQ0145).

Appendix A. Supplementary material

Supplementary data to this article can be found online at https://doi.org/10.1016/j.saa.2023.122650.

References

[1] S. Walter, J. Buchner, Molecular chaperones - Cellular machines for protein folding, Angewandte Chemie-International Edition 41 (7) (2002) 1098–1113.
[2] P.G. Wolynes, J.N. Onuchic, D. Thirumalai, Navigating the Folding Routes, Science 267 (5204) (1995) 1619–1620.
[3] T.L. Spires-Jones, J. Attems, D.R. Thal, Interactions of pathological proteins in neurodegenerative diseases, Acta Neuropathol. 134 (2) (2017) 187–205.
[4] D. Eisenberg, M. Jucker, The amyloid state of proteins in human diseases, Cell 148 (6) (2012) 1188–1203.
[5] T.P.J. Knowles, M. Vendruscolo, C.M. Dobson, The amyloid state and its association with protein misfolding diseases, Nat. Rev. Mol. Cell Biol. 15 (7) (2014) 384–396.
[6] M.C. Owen, D. Gnutt, M. Gao, et al., Effects of in vivo conditions on amyloid aggregation, Chem. Soc. Rev. 48 (14) (2019) 3946–3996.
[7] V.N. Uversky, A.L. Fink, Conformational constraints for amyloid fibrillation: the importance of being unfolded, Biochimica et Biophysica Acta (BBA)-Proteins and Proteomics 1698 (2) (2004) 131–153.
[8] M.C. Vaney, S. Maignan, M. Ries-Kautt, et al., High-resolution structure (1.33 Å) of a HEW lysozyme tetragonal crystal grown in the APCF apparatus. data and structural comparison with a crystal grown under microgravity from SpaceHab-01 mission, Acta Crystallogr. D Biol. Crystallogr. 52 (3) (1996) 505–517.
[9] L. Xing, K. Lin, X. Zhou, et al., Multistate mechanism of lysozyme denaturation through synchronous analysis of Raman spectra, J. Phys. Chem. B 120 (41) (2016) 10660–10667.
[10] L. Xing, W. Fan, N. Chen, et al., Amyloid formation kinetics of hen egg white lysozyme under heat and acidic conditions revealed by Raman spectroscopy, J. Raman Spectrosc. 50 (5) (2019) 629–640.
[11] L. Mariño, K. Pauwels, R. Casasnovas, et al., Ortho-methylated 3-hydroxypyridines hinder hen egg-white lysozyme fibrillogenesis, Sci. Rep. 5 (1) (2015) 1–14.
[12] S.A. Muthu, N. Mothi, S.M. Shiriskar, et al., Physical basis for the ofloxacin-induced acceleration of lysozyme aggregation and polymorphism in amyloid fibrils, Arch. Biochem. Biophys. 592 (2016) 10–19.
[13] W. Fan, L. Xing, N. Chen, et al., Promotion effect of succinimide on amyloid fibrillation of hen egg-white lysozyme, J. Phys. Chem. B 123 (38) (2019) 8057–8064.
[14] Y. Liu, M. Nguyen, A. Robert, et al., Metal Ions in Alzheimer’s Disease: a Key Role or Not? Acc. Chem. Res. 52 (7) (2019) 2026–2035.
[15] K.P. Kepp, Alzheimer’s disease: how metal ions define beta-amyloid function, Coord. Chem. Rev. 351 (2017) 127–159.
[16] F. Liu, Z. Zhang, L. Zhang, et al., Effect of metal ions on Alzheimer’s disease, Brain and Behavior 12 (3) (2022) e2527.
[17] H.M. Hussien, A. Abd-Elmegied, D.A. Ghareeb, et al., Neuroprotective effect of berberine against environmental heavy metals-induced neurotoxicity and Alzheimer’s-like disease in rats, Food Chem. Toxicol. 111 (2018) 432–444.

[18] P. Faller, C. Hureau, O. Berthoumieu, Role of metal ions in the self-assembly of the alzheimer's amyloid-beta peptide, Inorg. Chem. 52 (21) (2013) 12193–12206.
[19] M. Jureschi, A.V. Lupaescu, L. Ion, et al., Stoichiometry of heavy metal binding to peptides involved in alzheimer's disease: mass spectrometric evidence, Adv. Mass Spectrometry in Biomed. Res. 1140 (2019) 401–415.
[20] S. Ghosh, N.K. Pandey, S. Bhattacharya, et al., Fibrillation of hen egg white lysozyme triggers reduction of copper (II), Int. J. Biol. Macromol. 51 (1–2) (2012) 1–6.
[21] B. Ma, F. Zhang, X. Wang, et al., Investigating the inhibitory effects of zinc ions on amyloid fibril formation of hen egg-white lysozyme, Int. J. Biol. Macromol. 98 (2017) 717–722.
[22] J. Wawer, M. Szociński, M. Olszewski, et al., Influence of the ionic strength on the amyloid fibrillogenesis of hen egg white lysozyme, Int. J. Biol. Macromol. 121 (2019) 63–70.
[23] L. Xing, N. Chen, W. Fan, et al., Double-edged effects of aluminium ions on amyloid fibrillation of hen egg-white lysozyme, Int. J. Biol. Macromol. 132 (2019) 929–938.
[24] G. Notarachille, F. Arnesano, V. Calò, et al., Heavy metals toxicity: effect of cadmium ions on amyloid beta protein 1–42, *Possible implications for Alzheimer's disease.* Biometals 27 (2) (2014) 371–388.
[25] K.M. Bakulski, Y.A. Seo, R.C. Hickman, et al., Heavy metals exposure and alzheimer's disease and related dementias, J. Alzheimers Dis. 76 (4) (2020) 1215–1242.
[26] R. Chen, Q. Wang, J. Lv, et al., Multivariate correlation analysis of bio-accumulation with soil properties and potential health risks of cadmium and lead in rice seeds and cabbage in pollution zones, *China.* Environ. Geochem. Health 43 (9) (2021) 3485–3503.
[27] M. Zou, S. Zhou, Y. Zhou, et al., Cadmium pollution of soil-rice ecosystems in rice cultivation dominated regions in China: a review, Environ. Pollut. 280 (2021), 116965.
[28] M. Lu, X. Cao, J. Pan, et al., Identification of wheat (Triticum aestivum L.) genotypes for food safety on two different cadmium contaminated soils, Environ. Sci. Pollut. Res. 27 (8) (2020) 7943–7956.
[29] A.P. Sanders, B. Claus Henn, R.O. Wright, Perinatal and childhood exposure to cadmium, manganese, and metal mixtures and effects on cognition and behavior: a review of recent literature, Current environ. health reports 2 (3) (2015) 284–294.
[30] J. Min, K. Min, Blood cadmium levels and Alzheimer's disease mortality risk in older US adults, Environ. Health 15 (1) (2016) 1–6.
[31] R. Gupta, R.K. Shukla, A. Pandey, et al., Involvement of PKA/DARPP-32/PP1α and β-arrestin/akt/GSK-3β signaling in cadmium-induced DA-D2 receptor-mediated motor dysfunctions: protective role of quercetin, Sci. Rep. 8 (1) (2018) 1–18.
[32] Q. Peng, K.M. Bakulski, B. Nan, et al., Cadmium and Alzheimer's disease mortality in US adults: updated evidence with a urinary biomarker and extended follow-up time, Environ. Res. 157 (2017) 44–51.
[33] J. Wang, X. Yang, J. Wang, et al., Probing the binding interaction between cadmium(II) chloride and lysozyme, New J. Chem. 40 (4) (2016) 3738–3746.
[34] R. Olmo, M.D. Blanco, J.Ú.S.M. Socorro, et al., Effect of cadmium acetate on the conformation of lysozyme: functional implications, J. Enzym Inhib. 16 (1) (2001) 65–80.
[35] C. Wallin, S.B. Sholts, N. Österlund, et al., Alzheimer's disease and cigarette smoke components: effects of nicotine, PAHs, and Cd(II), Cr(III), Pb(II), Pb(IV) ions on amyloid-beta peptide aggregation, Sci. Rep. 7 (1) (2017) 1–14.
[36] D. Meleleo, C. Sblano, M.M. Storelli, et al., Evidence of cadmium and mercury involvement in the Aβ42 aggregation process, Biophys. Chem. 266 (2020), 106453.
[37] L. Jiang, T. Yao, Z. Zhu, et al., Impacts of Cd(II) on the conformation and self-aggregation of Alzheimer's tau fragment corresponding to the third repeat of microtubule-binding domain, Biochim. Biophys. Acta. 1774 (11) (2007) 1414–1421.
[38] E. Lorentzon, I. Horvath, R. Kumar, et al., Effects of the Toxic Metals Arsenite and Cadmium on α-Synuclein Aggregation In Vitro and in Cells, Int. J. Mol. Sci. 22 (21) (2021) 11455.
[39] T. Jacobson, S. Priya, S.K. Sharma, et al., Cadmium causes misfolding and aggregation of cytosolic proteins in yeast, Mol. Cell. Biol. 37 (17) (2017) e00490–e00516.
[40] O.S. Lee, V.I. Petrenko, K. Šipošová, et al., How fullerenes inhibit the amyloid fibril formation of hen lysozyme, J. Ind. Eng. Chem. 106 (2022) 168–176.
[41] H.R. Kalhor, A. Nazari Khodadadi, Synthesis and structure activity relationship of pyridazine-based inhibitors for elucidating the mechanism of amyloid inhibition, Chem. Res. Toxicol. 31 (10) (2018) 1092–1104.
[42] Y. Zou, Y. Li, W. Hao, et al., Parallel β-sheet fibril and antiparallel β-sheet oligomer: New insights into amyloid formation of hen egg white lysozyme under heat and acidic condition from FTIR spectroscopy, J. Phys. Chem. B 117 (15) (2013) 4003–4013.
[43] Y. Zou, W. Hao, H. Li, et al., New insight into amyloid fibril formation of hen egg white lysozyme using a two-step temperature-dependent FTIR approach, J. Phys. Chem. B 118 (33) (2014) 9834–9843.
[44] D. Kurouski, R.P. Van Duyne, I.K. Lednev, Exploring the structure and formation mechanism of amyloid fibrils by Raman spectroscopy: a review, Analyst 140 (15) (2015) 4967–4980.
[45] A. Downes, A. Elfick, Raman spectroscopy and related techniques in biomedicine, Sensors 10 (3) (2010) 1871–1889.
[46] G. Devitt, K. Howard, A. Mudher, et al., Raman Spectroscopy: an emerging tool in neurodegenerative disease research and diagnosis, ACS Chem. Nerosci. 9 (3) (2018) 404–420.
[47] N. Kuhar, S. Sil, T. Verma, et al., Challenges in application of Raman spectroscopy to biology and materials, RSC Adv. 8 (46) (2018) 25888–25908.
[48] Y. Zhang, P. S. Cremer, *The inverse and direct Hofmeister series for lysozyme.* Proceedings of the National Academy of Sciences, 2009, 106 36 p. 15249-15253.
[49] R. Majumdar, P. Manikwar, J.M. Hickey, et al., Effects of salts from the Hofmeister series on the conformational stability, aggregation propensity, and local flexibility of an IgG1 monoclonal antibody, Biochemistry 52 (19) (2013) 3376–3389.
[50] M. Xu, V.V. Ermolenkov, W. He, et al., Lysozyme fibrillation: deep UV Raman spectroscopic characterization of protein structural transformation, Biopolymers: Original Res. Biomolecules 79 (1) (2005) 58–61.
[51] N. Kuhar, S. Sil, S. Umapathy, Potential of Raman spectroscopic techniques to study proteins, Spectrochimica Acta Part a-Molecular and Biomolecular Spectroscopy 258 (2021), 119712.
[52] A.M. Herrero, P. Carmona, S. Cofrades, et al., Raman spectroscopic determination of structural changes in meat batters upon soy protein addition and heat treatment, Food Res. Int. 41 (7) (2008) 765–772.
[53] A.M. Herrero, M.I. Cambero, J.A. Ordóñez, et al., Raman spectroscopy study of the structural effect of microbial transglutaminase on meat systems and its relationship with textural characteristics, Food Chem. 109 (1) (2008) 25–32.
[54] M.C. Chen, R.C. Lord, R. Mendelsohn, Laser-excited raman-spectroscopy of biomolecules. 5. conformational-changes associated with chemical denaturation of lysozyme, J. Am. Chem. Soc. 96 (10) (1974) 3038–3042.
[55] J.A. Sweeney, S.A. Asher, Tryptophan Uv resonance raman excitation profiles, J. Phys. Chem. 94 (12) (1990) 4784–4791.
[56] S. Dolui, A. Mondal, A. Roy, et al., Order, disorder, and reorder state of lysozyme: aggregation mechanism by raman spectroscopy, J. Phys. Chem. B 124 (1) (2020) 50–60.
[57] V. Kocherbitov, J. Latynis, A. Misiunas, et al., Hydration of lysozyme studied by raman spectroscopy, J. Phys. Chem. B 117 (17) (2013) 4981–4992.
[58] H. Takeuchi, Raman structural markers of tryptophan and histidine side chains in proteins, Biopolymers: Original Res. Biomolecules 72 (5) (2003) 305–317.
[59] Z.Q. Wen, Raman spectroscopy of protein pharmaceuticals, J. Pharm. Sci. 96 (11) (2007) 2861–2878.
[60] I. Harada, T. Miura, H. Takeuchi, Origin of the doublet at 1360 and 1340 cm^{-1} in the Raman spectra of tryptophan and related compounds, Spectrochim. Acta A: Mol. Spectrosc. 42 (2–3) (1986) 307–312.
[61] T.J. Yu, J.L. Lippert, W.L. Peticola, Laser Raman Studies of Conformational Variations of Poly-L-Lysine, Biopolymers: Original Res. Biomolecules 12 (9) (1973) 2161–2176.
[62] K. Murayama, M. Tomida, Heat-induced secondary structure and conformation change of bovine serum albumin investigated by Fourier transform infrared spectroscopy, Biochemistry 43 (36) (2004) 11526–11532.
[63] M.J. Paquet, M. Laviolette, M. Pézolet, et al., Two-dimensional infrared correlation spectroscopy study of the aggregation of cytochrome c in the presence of dimyristoylphosphatidylglycerol, Biophys. J. 81 (1) (2001) 305–312.
[64] A. Barth, C. Zscherp, What vibrations tell about proteins, Q. Rev. Biophys. 35 (4) (2002) 369–430.
[65] I.H.M. Van Stokkum, H. Linsdell, J.M. Hadden, et al., Temperature-induced changes in protein structures studied by fourier-transform infrared-spectroscopy and global analysis, Biochemistry 34 (33) (1995) 10508–10518.
[66] A. Hedoux, J.F. Willart, R. Ionov, et al., Analysis of sugar bioprotective mechanisms on the thermal denaturation of lysozyme from Raman scattering and differential scanning calorimetry investigations, J. Phys. Chem. B 110 (45) (2006) 22886–22893.
[67] A. Hedoux, R. Ionov, J.F. Willart, et al., Evidence of a two-stage thermal denaturation process in lysozyme: a Raman scattering and differential scanning calorimetry investigation, J. Chem. Phys. 124 (1) (2006), 014703.
[68] W. Fan, X.D. Chen, L.M. Liu, et al., Concentration-dependent influence of silver nanoparticles on amyloid fibrillation kinetics of hen egg-white lysozyme, Chin. J. Chem. Phys. 34 (4) (2021) 393.
[69] P. Hanczyc, P. Fita, Laser emission of thioflavin T uncovers protein aggregation in amyloid nucleation phase, ACS Photonics 8 (9) (2021) 2598–2609.
[70] M. Biancalana, S. Koide, Molecular mechanism of Thioflavin-T binding to amyloid fibrils, Biochimica. Et Biophysica. Acta.-Proteins and Proteomics 1804 (7) (2010) 1405–1412.
[71] A. Biancardi, T. Biver, B. Mennucci, Fluorescent dyes in the context of DNA-binding: the case of Thioflavin T, Int. J. Quantum Chem. 117 (8) (2017) e25349.
[72] R. Mishra, Nicking and fragmentation are responsible for α-lactalbumin amyloid fibril formation at acidic pH and elevated temperature, Protein Sci. 30 (9) (2021) 1919–1934.